

ChemComm

Accepted Manuscript



This is an *Accepted Manuscript*, which has been through the Royal Society of Chemistry peer review process and has been accepted for publication.

Accepted Manuscripts are published online shortly after acceptance, before technical editing, formatting and proof reading. Using this free service, authors can make their results available to the community, in citable form, before we publish the edited article. We will replace this *Accepted Manuscript* with the edited and formatted *Advance Article* as soon as it is available.

You can find more information about *Accepted Manuscripts* in the [Information for Authors](#).

Please note that technical editing may introduce minor changes to the text and/or graphics, which may alter content. The journal's standard [Terms & Conditions](#) and the [Ethical guidelines](#) still apply. In no event shall the Royal Society of Chemistry be held responsible for any errors or omissions in this *Accepted Manuscript* or any consequences arising from the use of any information it contains.

COMMUNICATION

Charge-disproportionate ordered state with $\delta = 0.75$ in a chemically sensitive donor/acceptor $D^{\delta+}_2A^{2\delta-}$ layered framework†

Cite this: DOI: 10.1039/x0xx00000x

Received 00th January 2012,
Accepted 00th January 2012Hiroki Fukunaga,^a Takafumi Yoshino,^b Hajime Sagayama,^c Jun-ichi Yamaura,^d Takahisa Arima,^e Wataru Kosaka,^{f,a} and Hitoshi Miyasaka^{*f,a}

DOI: 10.1039/x0xx00000x

www.rsc.org/

A novel charge-disproportionation state with $\delta = 0.75$ was observed in an electron-donor (D)/-acceptor (A) $D^{\delta+}_2A^{2\delta-}$ layered framework by chemically tuning the electron-donating affinity of D at the boundary between $D^{0.5+}_2A^-$ and $D^+_2A^{2-}$ phases, which was pressure-sensitive via the formation of the $D^+_2A^{2-}$ oxidation state.

Tuning of the charge-ordered state in a multi-dimensional framework material, which enables the direct control of electrical and magnetic properties of a material, is a challenging theme in solid-state physical chemistry and materials chemistry. For achieving this purpose, two techniques are commonly available: chemical techniques, i.e. chemical doping or modification and physical techniques, i.e. switching by external stimuli such as temperature, pressure, electric field or photo-irradiation. Some molecular systems have indeed demonstrated intriguing properties associated with the fine-tuning of their charge-ordered state.¹⁻⁹ Among them, a family of metal-organic frameworks (MOFs) constructed from carboxylate-bridged paddlewheel-type diruthenium(II, II) complexes (abbreviated as $[\text{Ru}_2^{\text{II,II}}]$) and 7,7,8,8-tetracyanoquinodimethane (TCNQ) or *N,N*2-dicyanoquinonediimine (DCNQI) derivatives, as donor (D)/acceptor (A)-MOFs (D/A-MOFs), provides a good platform, where the electronic/magnetic properties of the MOFs are tuneable as a function of the charge-ordered state of the framework.^{3,8,9} A variety of oxidation states, including $D^0_2A^0$, $D^{0.5+}_2A^-$, and $D^+_2A^{2-}$, have been obtained in a D_2A -type MOF, which can be systematically manipulated through the on-demand choice of D and A components on the basis of the relationship of energy gap between HOMO level of D and LUMO level of A: $\Delta E_{\text{H-L}}(\text{DA}) = E_{\text{LUMO/A}} - E_{\text{HOMO/D}}$, with the neutral (N) state and the ionic (I) state as $\Delta E_{\text{H-L}}(\text{DA}) > 0$ and $\Delta E_{\text{H-L}}(\text{DA}) < 0$, respectively (Fig. S1a).⁹

When we examine the ionic state of the $[\text{Ru}_2]_2\text{TCNQ}$ compounds, i.e. D_2A -type compounds, with $\Delta E_{\text{H-L}}(\text{DA}) < 0$, two types of oxidation states, $D^{0.5+}_2A^-$ and $D^+_2A^{2-}$, which involve one-electron and two-electron transfers to A, respectively, can be considered. These oxidation states provide different magnetic ground states: the $D^{0.5+}_2A^-$ state generally undergoes long-range ordering through TCNQ^- with $S = 1/2$,⁸ whereas the $D^+_2A^{2-}$ state could lack

ordering or have weak ordering because of the presence of diamagnetic TCNQ^{2-} .¹⁰ Despite the same D_2A -type formulation and a common framework structure between them, these oxidation states should be alternated depending mainly on i) the electron-donation affinity of D vs. A used (i.e. the relationship between the ionisation potential of D and the electron affinity of A) and ii) the intrinsic on-site Coulomb repulsion (U) of the A species used. Given that the magnitude of U of TCNQ derivatives (TCNQR_x , $x = 2,5$ - or $2,3,5,6$ -R-substituted 7,7,8,8-tetracyano-*p*-quinodimethane; $\text{R}_x = \text{H}_4, \text{F}_2, \text{Cl}_2, \text{Br}_2, \text{F}_4, \text{Me}_2, (\text{OMe})_2$; BTDA-TCNQ = bis[1,2,5]dithiazolotetracyanoquinodimethane) is proportional to the potential difference between the first and second redox potentials of TCNQR_x ($|{}^2E_{1/2}(\text{A}) - {}^1E_{1/2}(\text{A})|$), the order of U for the TCNQR_x compounds is $\text{TCNQ}(\text{MeO})_2 < \text{TCNQMe}_2 < \text{BTDA-TCNQ} < \text{TCNQBr}_2 < \text{TCNQ} \approx \text{TCNQCl}_2 (\approx \text{DCNQIME}_2) < \text{TCNQF}_4 \approx \text{TCNQF}_2$ (Fig. S1b).^{9,10b} Specifically, U is the smallest in $\text{TCNQ}(\text{MeO})_2$ among this group; i.e. the energy window for $\Delta E_{\text{H-L}}(\text{DA})$, at which TCNQR_x^- is stably present, is 0.2–0.3 eV, which is much narrower than the window of 1.2–1.3 eV for TCNQF_4 or TCNQF_2 (Fig. S1b).^{10b} This result indicates that the oxidation state of the ionic state between $D^{0.5+}_2A^-$ and $D^+_2A^{2-}$ can be tuned via a small modification or perturbation induced by chemical and/or physical techniques when $\text{TCNQ}(\text{MeO})_2$ is used as A.

Here, we demonstrate charge control in layered D_2A systems with the $\text{TCNQ}(\text{MeO})_2$ acceptor by slightly changing the electron-donating ability of D through modification of the substitution position (e.g. *ortho*-, *meta*- and *para*-positions) of the fluorine group in $[\text{Ru}_2^{\text{II,II}}(x\text{-FPhCO}_2)_4]$ ($x\text{-FPhCO}_2^- = \text{ortho}$ -, *meta*- and *para*-fluorine substituted benzoate).¹¹ The present compounds are $\{[\text{Ru}_2(x\text{-FPhCO}_2)_4]_2\{\text{TCNQ}(\text{MeO})_2\}\} \cdot n(\text{solvent})$ ($x = \text{ortho}$, $n(\text{solvent}) = 4\text{CH}_2\text{Cl}_2$, **1**; $x = \text{meta}$, $n(\text{solvent}) = 4\text{CH}_2\text{Cl}_2$, **2**; $x = \text{para}$, $n(\text{solvent}) = 3\text{CH}_2\text{Cl}_2 \cdot \text{PhNO}_2$, **3**), in which the oxidation state was varied as $D^{0.5+}_2A^-$ for **1**, $D^+_2A^{2-}$ for **2**, and $D^{0.75+}_2A^{1.5-}$ for **3**. Herein, we focus on the novel charge-ordered state of $D^{0.75+}_2A^{1.5-}$ in **3**, in particular; this novel state was discovered in a superlattice comprising $[\text{Ru}_2^{\text{II,II}}]$, $[\text{Ru}_2^{\text{II,III}}]^+$, $\text{TCNQ}(\text{MeO})_2^-$ and $\text{TCNQ}(\text{MeO})_2^{2-}$ components in a formulation ratio of 1:3:1:1 caused by the disproportionation of intralayer electron transfers. This charge-ordered state can be regarded as an intermediate oxidation state between $D^{0.5+}_2A^-$ for **1** and $D^+_2A^{2-}$ for **2**.

All compounds were synthesised by a similar diffusion method of D/A units typically used in relevant compounds (see ESI). Infrared (IR) spectra of compounds are useful for confirming the oxidation state of component units,^{8c,12} which were measured by a microscopic technique using a single crystal coated with Paratone-N (HAMPTON Research, Inc.) to remove the effect caused by the elimination of crystallisation solvents. The $\nu(\text{C}\equiv\text{N})$ mode for all compounds was observed as red-shifted multiplets: 2109, 2158 and 2202 cm^{-1} for **1**; 2098(br), 2154 and 2190 cm^{-1} for **2**; and 2113(br), 2167, 2191(sh) and 2202 cm^{-1} for **3** (br = broad; sh = shoulder) (Fig. S2). These results indicate the reduced forms of $\text{TCNQ}(\text{MeO})_2$, where the one-electron reduced form ($\text{TCNQ}(\text{MeO})_2^{\cdot-}$) and two-electron reduced form ($\text{TCNQ}(\text{MeO})_2^{2-}$) are assigned for **1** and **2**, respectively, and their mixed modes are assigned for **3**.

Compounds **1** and **2**, which had the D_{2A} formulation, crystallised in the triclinic $P\bar{1}$ space group (#2), where two kinds of $[\text{Ru}_2]$ units and one $\text{TCNQ}(\text{MeO})_2$ unit are structurally characterised as an asymmetric unit, all of which have an inversion centre at the midpoint of the units, resulting in $Z = 1$ (Fig. S3; Table S1). The $\text{TCNQ}(\text{MeO})_2$ unit acts as a μ_4 -bridging ligand to coordinate to the axial sites of $[\text{Ru}_2]$ units, forming a two-dimensional ($2D$) fishnet-like network spreading over the (101) plane for **1** and over the (100) plane for **2** (Fig. 1 and Fig. S4) (the crystallisation solvent molecules are located at void spaces between layers). On the basis of the trend of $\text{Ru}-\text{N} = 2.22\text{--}2.23 \text{ \AA}$ for $[\text{Ru}_2^{\text{II,III}}]^+$ and $\text{Ru}-\text{N} = 2.27\text{--}2.28 \text{ \AA}$ for $[\text{Ru}_2^{\text{II,II}}]_2^{3,8,10}$ the oxidation state of $[\text{Ru}_2]$ units is suggested as $[\text{Ru}(1)_2^{\text{II,III}}]^+$ and $[\text{Ru}(2)_2^{\text{II,II}}]$ in **1** and as $[\text{Ru}_2^{\text{II,III}}]^+$ for both $[\text{Ru}_2]$ units in **2** (Tables S2 and S3). This charge assignment for $[\text{Ru}_2]$ units is supported by a more accurate indication based on a comparison of $\text{Ru}-\text{O}_{\text{eq}}$ bonds (O_{eq} = equatorial oxygen atoms): 2.06–2.07 \AA for $[\text{Ru}_2^{\text{II,II}}]$ and 2.02–2.03 \AA for $[\text{Ru}_2^{\text{II,III}}]^+$.^{9,13} In **1**, the average $\text{Ru}-\text{O}$ bond distances for $[\text{Ru}(1)_2]$ and $[\text{Ru}(2)_2]$ units are 2.027 and 2.068 \AA , respectively, indicating oxidation states of $[\text{Ru}(1)_2^{\text{II,III}}]^+$ and $[\text{Ru}(2)_2^{\text{II,II}}]$, respectively (Table S2). Meanwhile, in **2**, the average $\text{Ru}-\text{O}$ bond distances for both units are 2.023 and 2.026 \AA for $[\text{Ru}(1)_2]$ and $[\text{Ru}(2)_2]$, respectively, which are in the range for $[\text{Ru}_2^{\text{II,III}}]^+$ (Table S3).

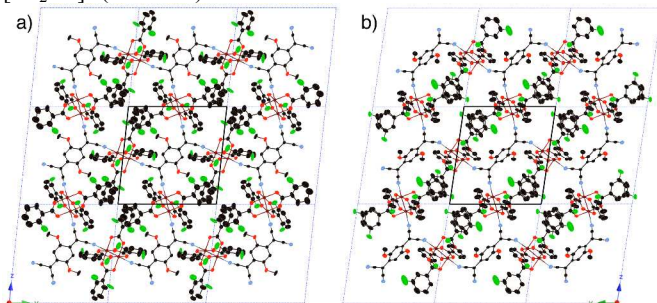


Fig. 1. D_{2A} layer structures of **1** (a) and **2** (b), where atoms of Ru, O, N, F and C are represented in brown, red, blue, green and black, respectively; the parallelogram indicates the unit cell.

Correspondingly, the oxidation state of $\text{TCNQ}(\text{MeO})_2^{2\delta-}$ is assigned as $\text{TCNQ}(\text{MeO})_2^{\cdot-}$ and $\text{TCNQ}(\text{MeO})_2^{2-}$ for **1** ($2\delta = 1.38$) and **2** ($2\delta = 2.20$), respectively, on the basis of the Kistenmacher relationship¹⁴ $2\delta = -\{A_p[c/(b+d)] + B_p\}$, in relation to TCNQ ($2\delta = 0$)¹⁵ and RbTCNQ ($2\delta = 1$)¹⁶ with $A_p = -41.667$ and $B_p = 19.833$ (the bond lengths b , c and d are respective bond distances for 7,9-, 1,7- and 1,2-positioned C–C sets in $\text{TCNQ}(\text{MeO})_2$, respectively) (Table S4). Specifically, the charge-ordered states for **1** and **2** can be written as $[\{\text{Ru}(1)_2^{5+}\}-\text{TCNQ}(\text{MeO})_2^{\cdot-}-\{\text{Ru}(2)_2^{4+}\}]_{\infty}$ and $[\{\text{Ru}(1)_2^{5+}\}-\text{TCNQ}(\text{MeO})_2^{2-}-\{\text{Ru}(2)_2^{5+}\}]_{\infty}$, respectively, leading to the conclusion that $1e^-$ and $2e^-$ transfer systems, respectively, occur in an identical D_{2A} system.

In the case of **3**, a similar unit cell in the triclinic $P\bar{1}$ space group and with a cell volume similar to that of **1** and **2** was considered; in this unit cell, two kinds of $[\text{Ru}_2]$ units and one $\text{TCNQ}(\text{MeO})_2$ unit with respective inversion centres were determined as an asymmetric unit with $Z = 1$ in an identical $2D$ layered fishnet-like network (ESI; Fig. S5; Table S1). This structural analysis is consistent with the charge assignment of $D^{0.75+}A^{1.5-}$ (see ESI); however, the presence of such a half-value of charge presupposes three possible patterns of charge state in the D_{2A} system: i) a delocalised charge distributed state, ii) a charge randomly ordered state as a steady state and iii) a novel charge-ordered state with a superlattice as a steady state. In the present case, model (iii) was adopted because diffraction spots indicating the half-index value for the c -axis $q = (0, 0, 1/2)$ were observed when X-ray diffraction spots were carefully measured (Fig. 2a), which demonstrates the occurrence of unit-cell doubling such that the c -axis is twice as large as the original minimum cell with $Z = 1$.

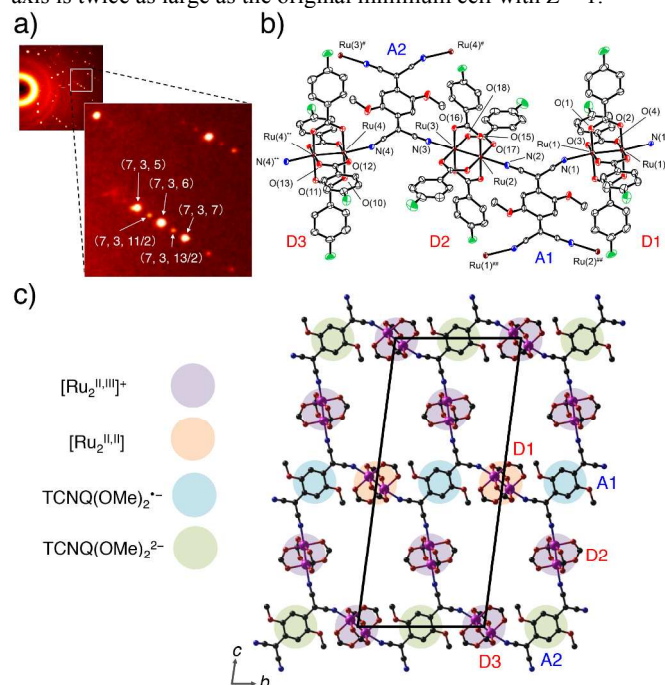


Fig. 2. Structure of **3**. a) Diffraction spots on a single-crystal X-ray oscillation photograph taken at 100 K. b) Structure of the formula unit (50% probability ellipsoids), where the symmetry operations are: *) $-x+2, -y, -z+1$; **) $-x, -y+2, -z$; #) $-x+1, -y+1, -z$; ##) $-x+1, -y+1, -z+1$ and where hydrogen atoms are omitted for clarity. c) A packing view in the superlattice projected along the a -axis (the parallelogram indicates the superlattice unit cell), where the aromatic group (p -FPh) of $[\text{Ru}_2]$ units and hydrogen atoms are omitted for clarity. The coloured circles represent the charge of the units.

In the superlattice, three types of $[\text{Ru}_2]$ units (D1, D2 and D3 in Fig. 2b) and two types of $\text{TCNQ}(\text{MeO})_2$ units (A1 and A2 in Fig. 2b) are structurally identified, where D1 and D3 and both $\text{TCNQ}(\text{MeO})_2$ units (A1 and A2) have an inversion centre at the midpoint of the respective units, whereas all atoms of D2 are determined as an asymmetric unit; hence, the unit cell has $Z = 2$. The average $\text{Ru}-\text{O}_{\text{eq}}$ length is 2.064, 2.025 and 2.027 \AA for D1–D3, respectively (Table S5); D2 and D3 are assigned to $[\text{Ru}_2^{\text{II,III}}]^+$, whereas D1 is $[\text{Ru}_2^{\text{II,II}}]$. The $\text{Ru}-\text{N}$ lengths agree with these assignments, although the $\text{Ru}(2)-\text{N}(2)$ bond (2.256(4) \AA) was observed as an intermediate value for between $[\text{Ru}_2^{\text{II,II}}]$ and $[\text{Ru}_2^{\text{II,III}}]^+$ (Table S5). The Kistenmacher analysis on the two $\text{TCNQ}(\text{MeO})_2$ moieties (A1 and

A2) resulted in $2\delta = 1.13$ and 2.08, respectively (Table S4). These charge assignments are in good agreement with the averaged charge distribution of $D^{0.75+}_2A^{1.5-}$.

Figure 2c depicts a packing view projected along the a -axis, showing a 2-D fishnet-like network similar to those of **1** and **2** (the projection from another direction is given in Fig. S6). The $[Ru_2^{II,III}]$ (D1) species alternately appears with $[Ru_2^{II,III}]^+$ of D3 along the c -axis. Following this rule, the $TCNQ(MeO)_2^{2-}$ (A1) species alternately appears with $TCNQ(MeO)_2^{2-}$ (A2), making a set of D1–A1 and D3–A2 along the b -axis direction. The D2 units with $[Ru_2^{II,III}]^+$ connect these sets along the c -axis to form a 2-D network. Thus, the two types of charge arrangements, $D^{0.5+}_2A^{2-}$ moieties, alternately appear along the c -axis direction; to the best of our knowledge, this system represents the first time that such an unusual charge-ordered state due to the disproportionation of charge in a 2-D framework has been observed.

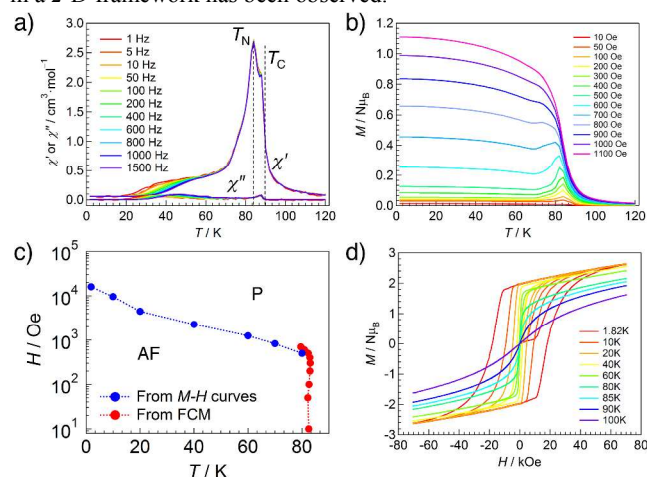


Fig. 3. Magnetic properties of **1**. a) Temperature dependence of ac susceptibilities (χ' : in-phase; χ'' : out-of-phase) measured at zero dc field and under a 3 Oe oscillating field. b) Field-cooled magnetization (FCM) curves measured at several different field intensities. c) An H - T phase diagram, where AF and P indicate antiferromagnetic and paramagnetic phases, respectively. d) Field dependence of the magnetization measured at several temperatures.

The magnetic state of the present $[Ru_2]_2TCNQ$ system is variable, depending on the charge-ordered states; spin components of $[Ru_2^{II,III}]$ ($S = 1$) and $[Ru_2^{II,III}]^+$ ($S = 3/2$) possess strong magnetic anisotropy,¹⁷ whereas $TCNQ^0$ and $TCNQ^{2-}$ are diamagnetic and $TCNQ^-$ ($S = 1/2$) is paramagnetic. In addition, the magnetic exchange coupling (J) between $[Ru_2^{II,III}]^+/[Ru_2^{II,III}]$ and $TCNQ^-$ is known to be very strong, often exceeding 100 K with the support of $A^- \rightarrow D^+$ low-energy charge transfer.^{3,9} Furthermore, the magnetically ordered state in such low-dimensional D_2A systems is strongly affected by interlayer environments associated with interlayer dipole interactions.⁸

Compound **1** shows a typical magnetic behaviour predicted from the $[\{Ru(1)_2^{5+}\}-TCNQ(MeO)_2^{2-}-\{Ru(2)_2^{4+}\}]_\infty$ charge-ordered state,⁸ which undergoes long-range magnetic ordering that is explained by intralayer ferrimagnetic ordering at $T_C = 88$ K followed by interlayer antiferromagnetic ordering at $T_N = 83$ K (Fig. 3a and Fig S7 show the ac susceptibility and temperature dependence of the magnetic susceptibility (χ) and χT product of **1** measured at 1 kOe, respectively). Notably, **1** indeed locates at an antiferromagnetic ground state under the field-cooling condition (Fig. 3b; Fig. 3c shows a phase diagram of **1**), but maintains a ferrimagnetic state after undergoing a transition to this state under an applied magnetic field, even at temperatures below the T_N , indicating the occurrence

of field-induced ferrimagnetic transition. Actually, typical hysteresis curves were observed in the magnetization (M) vs. H plots obtained under effective coercive fields at temperatures up to the T_N (Fig. 3d).

Compound **2** exhibits the $[\{Ru(1)_2^{5+}\}-TCNQ(MeO)_2^{2-}-\{Ru(2)_2^{5+}\}]_\infty$ charge-ordered state, which provides a homo-spin paramagnetic system with $S = 3/2$; this paramagnetic system arises from $[Ru_2^{II,III}]^+$ isolated by diamagnetic $TCNQ(MeO)_2^{2-}$ units. This spin state predicts a monotonic decrease of χT because of magnetic anisotropy (zero-field splitting: ZFS) of $[Ru_2^{II,III}]^+$ with decreasing temperature.¹⁰ Indeed, the χT product gradually decreases upon cooling from 300 K, as expected, but suddenly increases at approximately 80 K, exhibits small bump with a peak at 61 K, decreases monotonically to 1.8 K (Fig. S8a). This bump in the χT - T plot could be due to the presence of small domains formed by partial solvent eliminations, where the $[Ru_2^{II,III}]^+$ spins with $S = 3/2$ are strongly interacting through $TCNQ(MeO)_2^{2-}$ and/or $TCNQ(MeO)_2^-$ are partially formed via inverse electron transfer. Actually, the increase in the magnetization was enhanced when the temperature sweep was repeated between 300 K and 1.8 K in vacuo (Fig. S8b); the dried sample of **2** exhibited long-range order at 70 K (Fig. S9). Thus, the essential magnetic behaviour of **2** originates from the $[\{Ru(1)_2^{5+}\}-TCNQ(MeO)_2^{2-}-\{Ru(2)_2^{5+}\}]_\infty$ charge-ordered state, where the decrease of χT (Fig. S8a) is mainly due to the effect of ZFS of the $[Ru_2^{II,III}]^+$ units.

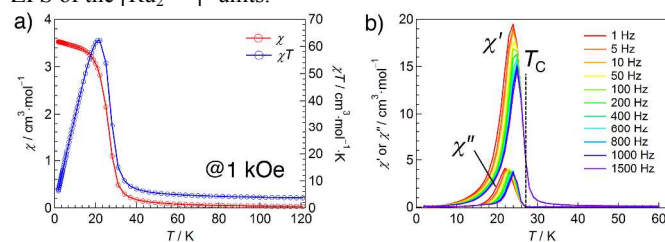


Fig. 4. Magnetic properties of **3**. a) Temperature dependence of χ and χT measured at 1 kOe. b) Temperature dependence of ac susceptibilities measured at zero dc field and under a 3 Oe oscillating field.

The unique charge-ordered state of **3** has two types of $TCNQ(MeO)_2$, i.e. $TCNQ(MeO)_2^-$ and $TCNQ(MeO)_2^{2-}$, which are surrounded by two $[Ru_2^{II,III}]$ units and two $[Ru_2^{II,III}]^+$ units for $TCNQ(MeO)_2^-$, as in **1**, and four $[Ru_2^{II,III}]^+$ units for $TCNQ(MeO)_2^{2-}$, as in **2**, respectively. These situations alternately occur along the c -axis, which appears to be an intermediate state between the $1e^-$ and $2e^-$ transfer states, i.e. intermediate between **1** and **2**. The χ measured at 1 kOe, $1.15 \times 10^{-4} \text{ cm}^3 \text{ mol}^{-1}$ at 300 K, gradually increases as the temperature is decreased to approximately 30 K and then abruptly increases without any peak as the temperature is decreased to 1.8 K ($3.53 \times 10^{-4} \text{ cm}^3 \text{ mol}^{-1}$ at 1.8 K) (Fig. 4a); this basic behaviour is common at lower fields applied at 3 Oe (Fig. S10). The χT products increase without showing a minimum and abruptly increase at ca. 30 K to reach a maximum at 22 K, followed by a decrease (Fig. 4a). Thus, the $[Ru_2]$ units through $TCNQ(MeO)_2^-$ are, at least, ferrimagnetically arranged with a strong coupling constant, as in **1**, and the formed domains can be weakly ferromagnetically ordered through isolated $S = 3/2$ spins around $TCNQ(MeO)_2^{2-}$ and/or through space between layers. The ac susceptibilities revealed the presence of long-range ordering at 27 K with a weak frequency dependence ($\phi < 0.1$ from $\phi = \Delta T / T\Delta(\log\omega)$) (Fig. 4b),¹⁸ even though their peaks are monotonic and sharp, suggesting that the movement of domain walls should be relatively slow. The M - H curves measured at several temperatures between 1.8 K and 30 K show a hysteresis; however, the magnetization value at 7 T ($1.35 \mu_B$) is considerably smaller than that for **1** ($2.63 \mu_B$)

(Fig. S11). The remnant magnetization value is also small in the same temperature range. In addition, the coercive field is smaller than that for **1**; rather, the hysteresis loop for **3** resembles a miniature version of that for **1**. This behaviour can be explained by an alternating arrangement of strongly coupled ferrimagnetic domains via $\text{TCNQ}(\text{MeO})_2^{\cdot-}$ and weakly coupled paramagnetic species around diamagnetic $\text{TCNQ}(\text{MeO})_2^{2-}$ moieties.

An ‘intermediate’ oxidation state such as that observed in **3** could trigger a phase transition to another stabilised oxidation state (e.g. $\text{D}^+_{2}\text{A}^{2-}$, as observed in **2**) induced by an external stimulus such as pressure. Hydrostatic pressures up to 7.34 kbar were applied to **3** using a piston-cylinder-type cell fabricated from a Cu–Be alloy, in conjunction with a Pb probe.^{19–21} The magnetization at low temperatures, which increases steeply at approximately $T_C = 27$ K, gradually decreased with increasing pressure and almost disappeared at $P = 3$ kbar, suggesting a transition to a paramagnetic state (Fig. 5a). This behaviour was confirmed by the M – H curve measured at 1.8 K: the hysteresis curve of **3** disappeared at $P = 3$ kbar (Fig. 5b). The final M – H feature is almost linear, typical for a paramagnetic $[\text{Ru}_2^{\text{II,III}}]^+$ species. Thus, the application of pressure to **3** successfully changed its oxidation state from $\text{D}^{0.75+}_2\text{A}^{1.5-}$ to $\text{D}^+_{2}\text{A}^{2-}$. Notably, the original state of **3** was almost recovered when the pressure was released.

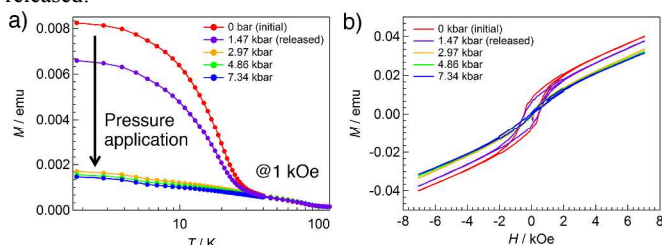


Fig. 5. Pressure-induced changes in the magnetization of **3**, as observed in M – T (a) and M – H (b) curves.

In summary, following the prediction based on the ionisation diagram of $\Delta E_{\text{H-L}}(\text{DA})$ vs. $({}^2E_{1/2}(\text{A}) - {}^1E_{1/2}(\text{A}))$ (Fig. S1b),^{9,10b} D/A sets at around the boundary between $\text{D}^{0.5+}_2\text{A}^-$ and $\text{D}^+_{2}\text{A}^{2-}$ were investigated; consequently, three types of charge-transferred-state $\text{D}^{\delta+}_2\text{A}^{2\delta-}$ with $\delta = 0.5, 1$ and 0.75 for **1–3**, respectively, were rationally obtained through modification of the position of the F substituent (i.e. either *o*-, *m*- or *p*-) of $[\text{Ru}_2^{\text{II,III}}(x\text{-FPhCO}_2)_4]$ as D, respectively. Compound **3** has a novel charge-ordered state—a superlattice comprising $[\text{Ru}_2^{\text{II,III}}]$, $[\text{Ru}_2^{\text{II,III}}]^+$, $\text{TCNQ}(\text{MeO})_2^{\cdot-}$ and $\text{TCNQ}(\text{MeO})_2^{2-}$ components in a formulation ratio of 1:3:1:1—caused by the disproportionation of intralayer electron transfers. This oxidation state appears to be an intermediate state between $\text{D}^{0.5+}_2\text{A}^-$ and $\text{D}^+_{2}\text{A}^{2-}$. This unique charge-ordered state is sensitive to applied pressure and changes into $\text{D}^+_{2}\text{A}^{2-}$, demonstrating that the charge-ordered states in D/A frameworks are flexibly controllable via the application of adequate external stimuli. Thus, D/A-MOFs have a strong potential for the design of molecular electronic/magnetic devices with multiple tunability via external stimuli.

We thank Keiko Kubo (Tohoku University) for her assistance in synthesising compounds. A portion of the X-ray diffraction study was performed using the facilities of the Institute for Solid State Physics, the University of Tokyo. This work was supported by a Grant-in-Aid for Scientific Research (No. 24245012) and on Innovative Areas (‘Coordination Programming’ Area 2107, No. 24108714) from the MEXT of Japan, the ICC-IMR project, the LC-IMR project and the Asahi Glass Foundation.

Notes and references

^a Department of Chemistry, Graduate School of Science, Tohoku University, Aramaki-Aza-Aoba, Aoba-ku, Sendai 980-8578, Japan

^b Department of Chemistry, Division of Material Sciences, Graduate School of Natural Science and Technology, Kanazawa University, Kakuma-machi, Kanazawa 920-1192, Japan

^c Institute of Materials Structure Science, High Energy Accelerator Research Organization, Tsukuba, Ibaraki 305-0801, Japan

^d Materials Research Center for Element Strategy, Tokyo Institute of Technology, Yokohama, Kanagawa 226-8503, Japan

^e Department of Advanced Materials Science, The University of Tokyo, Kashiwa 277-8561, Japan

^f Institute for Materials Research, Tohoku University, 2-1-1 Katahira, Aoba-ku, Sendai 980-8577, Japan. E-mail: miyasaka@imr.tohoku.ac.jp

[†] Electronic supplementary information (ESI) available: Details of experiments, techniques, and structures; Table S1–S6, Fig. S1–S11. For ESI and crystallographic data in CIF or other electronic format see DOI: .

- 1 Y. Iwasa, E. Funatsu, T. Hasegawa, T. Koda and M. Yamashita, *Appl. Phys. Lett.*, 1991, **59**, 2219.
- 2 S. Takaishi, M. Takamura, T. Kajiwara, H. Miyasaka, M. Yamashita, M. Iwata, H. Matsuzaki, H. Okamoto, H. Tanaka, S. Kuroda, H. Nishikawa, H. Oshio, K. Kato and M. Takata, *J. Am. Chem. Soc.*, 2008, **130**, 12080.
- 3 (a) H. Miyasaka, N. Motokawa, T. Chiyo, M. Takemura, M. Yamashita, H. Sagayama and T. Arima, *J. Am. Chem. Soc.*, 2011, **133**, 5338; (b) K. Nakabayashi and H. Miyasaka, *Chem. Eur. J.*, 2014, **20**, 5121.
- 4 N. Hoshino, F. Iijima, G. N. Newton, N. Yoshida, T. Shiga, H. Nojiri, A. Nakao, R. Kumai, Y. Murakami and H. Oshio, *Nat. Chem.*, 2012, **4**, 921.
- 5 J. B. Torrance, J. E. Vazquez, J. J. Mayerle and V. Y. Lee, *Phys. Rev. Lett.*, 1981, **46**, 253.
- 6 (a) H. Okamoto, T. Mitani, Y. Tokura, S. Koshihara, T. Komatsu, Y. Iwasa, T. Koda and G. Saito, *Phys. Rev. B*, 1991, **43**, 8224; (b) S. Horiuchi, Y. Okimoto, R. Kumai and Y. Tokura, *J. Am. Chem. Soc.*, 2001, **123**, 665; (c) S. Horiuchi and Y. Tokura, *Nat. Mater.*, 2008, **7**, 357; (d) F. Kagawa, S. Horiuchi, M. Tokunaga, J. Fujioka and Y. Tokura, *Nat. Phys.*, 2010, **6**, 169.
- 7 J. S. Miller and A. J. Epstein, *Angew. Chem., Int. Ed.*, 1994, **33**, 385.
- 8 (a) H. Miyasaka, T. Izawa, N. Takahashi, M. Yamashita, K. R. Dunbar, *J. Am. Chem. Soc.*, 2006, **128**, 11358; (b) N. Motokawa, T. Oyama, S. Matsunaga, H. Miyasaka, M. Yamashita and K. R. Dunbar, *CrystEngComm*, 2009, **11**, 2121; (c) H. Miyasaka, N. Motokawa, S. Matsunaga, M. Yamashita, K. Sugimoto, T. Mori, N. Toyota and K. R. Dunbar, *J. Am. Chem. Soc.*, 2010, **132**, 1532; (d) K. Nakabayashi, M. Nishio, K. Kubo, W. Kosaka and H. Miyasaka, *Dalton Trans.*, 2012, **41**, 6072; (e) N. Motokawa, S. Matsunaga, S. Takaishi, H. Miyasaka, M. Yamashita and K. R. Dunbar, *J. Am. Chem. Soc.*, 2010, **132**, 11943.
- 9 H. Miyasaka, *Acc. Chem. Res.*, 2013, **46**, 248.
- 10 (a) H. Miyasaka, T. Morita and M. Yamashita, *Chem. Commun.*, 2011, **47**, 271; (b) K. Wataru, T. Morita, T. Yokoyama, J. Zhang and H. Miyasaka, *Inorg. Chem.*, 2015, **54**, 1518.
- 11 H. Miyasaka, N. Motokawa, R. Atsumi, H. Kamo, Y. Asai and M. Yamashita, *Dalton Trans.*, 2011, **40**, 673.
- 12 K. Nakamoto, *Infrared and Raman Spectra of Inorganic and Coordination Compounds*, 6th ed.; Wiley-Interscience: New York, 2009.
- 13 F. A. Cotton and R. A. Walton, *Multiple Bonds between Metal Atoms*, second ed., Oxford University Press, Oxford, 1993.
- 14 T. J. Kistenmacher, T. J. Emge, A. N. Bloch and D. O. Cowan, *Acta Crystallogr., Sect. B* **1982**, **38**, 1193.
- 15 R. E. Long, R. A. Sparks and K. N. Trueblood, *Acta Crystallogr.*, 1965, **18**, 932.
- 16 A. Hoekstra, T. Spoelder and A. Vos, *Acta Crystallogr. Sect. B*, 1972, **28**, 14.
- 17 M. A. S. Aquino, *Coord. Chem. Rev.*, 1998, **170**, 141.
- 18 J. A. Mydosh, *Spin Glasses*; Taylor and Francis: Washington, DC, 1993; Chapter 3.
- 19 N. Motokawa, H. Miyasaka and M. Yamashita, *Dalton Trans.*, 2010, **39**, 4724.
- 20 M. Mito, *J. Phys. Soc. Jpn. Suppl. A*, 2007, **76**, 182.
- 21 H. Fukunaga and H. Miyasaka, *Angew. Chem. Int. Ed.*, 2015, **54**, 569.